Hindawi
Journal of Nanomaterials
Volume 2021, Article ID 9959552, 11 pages
https://doi.org/10.1155/2021/9959552

Research Article

Nanoparticles of γ-Sitoesterol and Ag on Clinoptilolite Zeolites

Miguel Angel Hernandez,[1] **Martha Alicia Salgado**,[2] **Roberto Portillo**,[2] **Vitalii Petranovskii**,[3] **Gabriela Itzel Hernández**,[4] **Deisy Santamaria**,[5] **and Efrain Rubio**[6]

[1]*Departamento de Investigación en Zeolitas y Posgrado en Agroecología, Instituto de Ciencias de la Universidad Autonoma de Puebla, Edif IC12, Ciudad Universitaria, 72570 Puebla, Mexico*
[2]*Facultad de Ciencias Químicas, Universidad Autonoma de Puebla, Mexico*
[3]*Centro de Nanociencias y Nanotecnología, UNAM, B.C., Norte, Ensenada, Mexico*
[4]*Universidad Autonoma Metropolitana-Iztapalapa, Av. San Rafael Atlixco No. 186, Col. Vicentina, 09340 Iztapalapa, Mexico*
[5]*Facultad de Ingeniería Química, Universidad Autonoma de Puebla, Mexico*
[6]*Dirección de Innovación y Transferencia de Tecnología, Universidad Autonoma de Puebla, Mexico*

Correspondence should be addressed to Miguel Angel Hernandez; vaga1957@gmail.com

Received 23 March 2021; Revised 27 May 2021; Accepted 27 June 2021; Published 19 July 2021

Academic Editor: P. Davide Cozzoli

This work reports, the obtainment and stabilization of organic nanoparticles (γ-sitosterol) and Ag cations on the external area of Ca-clinoptilolite zeolite (Z17) are presented. The novelty of the present study lies in the formation and stabilization of nanoparticle organic molecules (γ-sitosterol) and inorganic cations (Ag) on the external area of Ca-clinoptilolite zeolite. The γ-sitosterol nanoparticles were obtained using *Tournefortia hirsutissima* and were later stabilized on the external area of Ca-clinoptilolite. The Ca-clinoptilolite-rich mineral as well as silver zeolitic minerals was characterized by using X-ray diffraction (XRD) and scanning electron microscopy (SEM); elementary composition of the zeolitic mineral was determined by microanalyses (EDS) and high-resolution adsorption (HRADS) using N_2 adsorption as a probe molecule. The EDS results about the exchange with Ag indicate the following sequence: Z17Ag03 > Z17Ag-09 > Z17Ag-06 > Z17Ag-01. The XRD studies indicate that only in the sample Z17Ag-03 there is an average crystal size of nanoparticles formed of 45.387 nm as determined by Sherrer's equation. SEM images of clinoptilolite showed the presence of crystals with irregular and poorly defined box shapes that are typical for this type of zeolites. The nanoporosity of natural zeolites was studied by N_2 adsorption; external areas were estimated through the De Boer and BET equations. The specific surface area calculated by BET equation, A_{SB}, presents the following sequence: γ-SZ17 > Z17 > Z17Ag09 > Z17Ag03 > Z17Ag01 > Z17Ag06, while for the values of the external area obtained by the *t* method, the sequence is A_{ST}: γ-Z17 > Z17 > Z17Ag03 > z17Ag09 > Z17Ag06 > Z17Ag01. For its part, the pore size distributions tell us that the sample Z17 exhibits a sharp multimodal distribution with pore size maxima happening at 1.262, 1.933, 3.824, and 4.282 nm. Z17Ag01 exhibits a bimodal distribution with pore size maxima occurring at 5.45 and 5.533 nm. The sample Z17Ag06 exhibits a sharp bimodal distribution with pore size maxima happening at 3.666 and 7.021 nm, and the sample Z17Ag09 exhibits a sharp trimodal distribution with pore size maxima happening at 1.853, 4.275 and 5.967 nm. Antibacterial activities of the exchanged samples with Ag on the external surface area were measured as a function of exchange level against Gram-positive bacteria (*P. aureoginosa*, *K. pneumonie*, *and A. baumannii*) and Gram-negative bacteria (*E. coli*, *S. saprophyticcus*, *S. aureus*, and *E. feacalis*); the selectivity sequence of the clinoptilolite and antibacterial activity results are presented. Z17Ag09 clinoptilolite seemed to be a promising antibacterial material.

1. Introduction

Diabetes mellitus (DM) is a disease known for its multiple complications, one of them being the diabetic foot [1]. There is a great interest in the development of materials with reliable and environmentally friendly microbicidal action to counteract the effects of this disease. Metals and their cations such as silver (Ag), zinc (Zn), copper (Cu), mercury (Hg),

cadmium (Cd), chromium (Cr), and lead (Pb) can be used in a variety of ways as antimicrobial agents. Among these metals, Ag and Zn have long been used in medicines. The antibacterial activity of Ag is well known, it has an inhibitory effect on the growth of bacteria and retains its activity for a long time; also, there is no risk of developing bacterial resistance [2]. With the development of fabrication strategies for novel nanomaterials and nanostructures, Ag-loaded nanocomposites have been regarded as a very broad-spectrum antimicrobial agent, which can encourage their potential applications in various fields excelling in very specific areas such as biomedicine, food preservation, and water purification [3]. Among the diverse metal nanoparticles, it is silver nanoparticles (AgNPs) that have become very important and most frequently used [4]. The biocidal effect of AgNPs mainly depends on the type of bond that exists and the subsequent release of silver ions. To enhance their bactericidal properties, AgNPs require suitable substrates that are compatible with their bactericidal properties. The resulting AgNPs agents exhibit excellent antibacterial properties when chosen well. It is noted that their antimicrobial activities increase with decreasing particle size. The mechanism of action is explained by damage to the membrane of the bacterial cell, which causes leakage of the cytoplasm. In addition, two types of action mechanisms are considered, i. e., contact action and release of Ag^+, which are responsible for the antimicrobial effect of AgNPs [5, 6]. In order to enhance their bactericidal effect, AgNps require suitable carriers that are compatible with their properties. Therefore, the design and fabrication of novel Ag-nanostructures suitable for such purposes are necessary to open up new possibilities with this type of cations and Ag nanoparticles and to obtain complex materials that act as an effective antibacterial agent. To date, various nanocomposite materials have been proposed, into which Ag is being incorporated; among them, nanocomposite Ag-graphene, nanocomposites based on Ag-oxide, Ag-macromolecules, and Ag-zeolites (AgZ) are known [7]. The nanoporous lattice of the zeolite allows metal cations to move freely, and this apparently is responsible for their activity toward microorganisms [8]. One of the best known and most frequently used zeolites to perform ion exchange treatments with bactericidal cations is clinoptilolite. Clinoptilolite (framework-type HEU) is a hydrophilic zeolite and has a three-dimensional three-channel system, filled by cations and water molecules (Figure 1) [9]. Natural zeolites are complex adsorption systems, since in addition to micropores, they also have mesopores and macropores [10]. In similar samples, A. Semra and U. Semra [11] studied the bactericidal activity of different types of exchangeable cations in a clinoptilolite. For his part, Dimova et al. [12] have studied exchanged Ag-clinoptilolite through Rietveld structural refinement and three independent Ag sites were located in channels of the clinoptilolite structure. At the same time, Concepcion-Rosabal et al. and Rodriguez-Fuentes et al. discussed the characteristics of Ag-clinoptilolites (natural and synthetic) containing Ag in various states. Many of the results obtained using modified zeolites have been applied and published in available patents [13, 14]. Also, Bogdanchikova et al. [15, 16] have presented a literature review regarding the reexamination of the structure and composition of Ag-clinoptilolite and its applications as antibacterial agent.

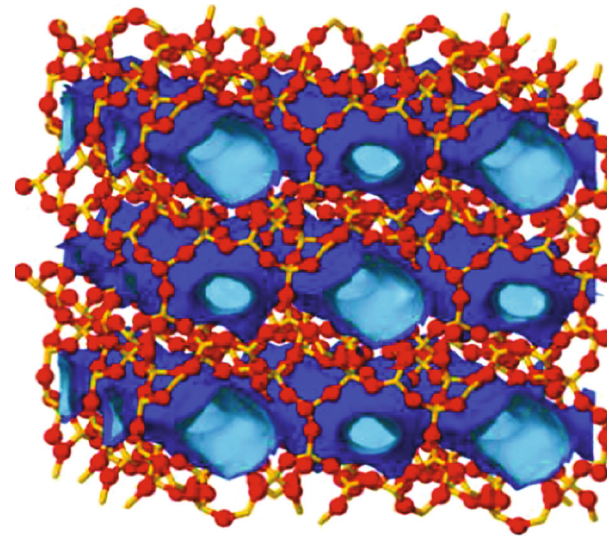

Figure 1: Clinoptilolite structure, International Zeolite Association/Structure (http://izasc.ethz.ch/fmi/xsl/IZA-SC/ft.xsl), the Si and O ions (yellow and red), and the inner surface (blue) of the channels are shown.

Pavelic et al. [17] analyzed the scientific literature on the health effects and safety of various clinoptilolite-based materials for medical use; they have proposed some complex, science-based hypotheses about possible biological mechanisms underlaying the observed effects on the health and body homeostasis. Colella [18, 19] reviewed the biomedical and veterinary applications of natural zeolites. Cerria et al. [20] carried out very relevant works on zeolites exchanged with Zn and their applications in antiacne therapies. On the other hand, another very important compound is γ-sitosterol, which is used to accelerate the healing process of the diabetic foot, as it reduces hyperglycemia, increases insulin secretion, and inhibits glucogenesis [21]. Many authors propose to develop a protein antidiabetic drug. Oral administration of γ-sitosterol in induced diabetic rats resulted in a significant decrease in blood glucose and glycosylated hemoglobin with a significant increase in plasma insulin level, body weight, and food intake [21, 22].

The purpose of this work is to obtain a group of materials based on γ-sitoesterol-clinoptilolite (γ-SZ17) and Ag-clinoptilolite (Z17AgX) with a number of emerging pores created during the ion exchange process. To do this, the γ-SZ17 will be mixed in alcoholic solutions with Z17Ag, previously prepared at 3 different concentrations; thereafter, specific ion exchange time protocols have been followed. The experimental techniques employed to characterize Z17AgX clinoptilolite susbtrates include X-ray diffraction (XRD), scanning electron microscopy (SEM), energy dispersive X-ray spectroscopy (EDS), and high-resolution adsorption (HRADS).

2. Experimental Section

2.1. Materials. γ-Sitosterol-clinoptilolite (γ-SZ17) was synthesized, purified, and characterized in a manner similar to

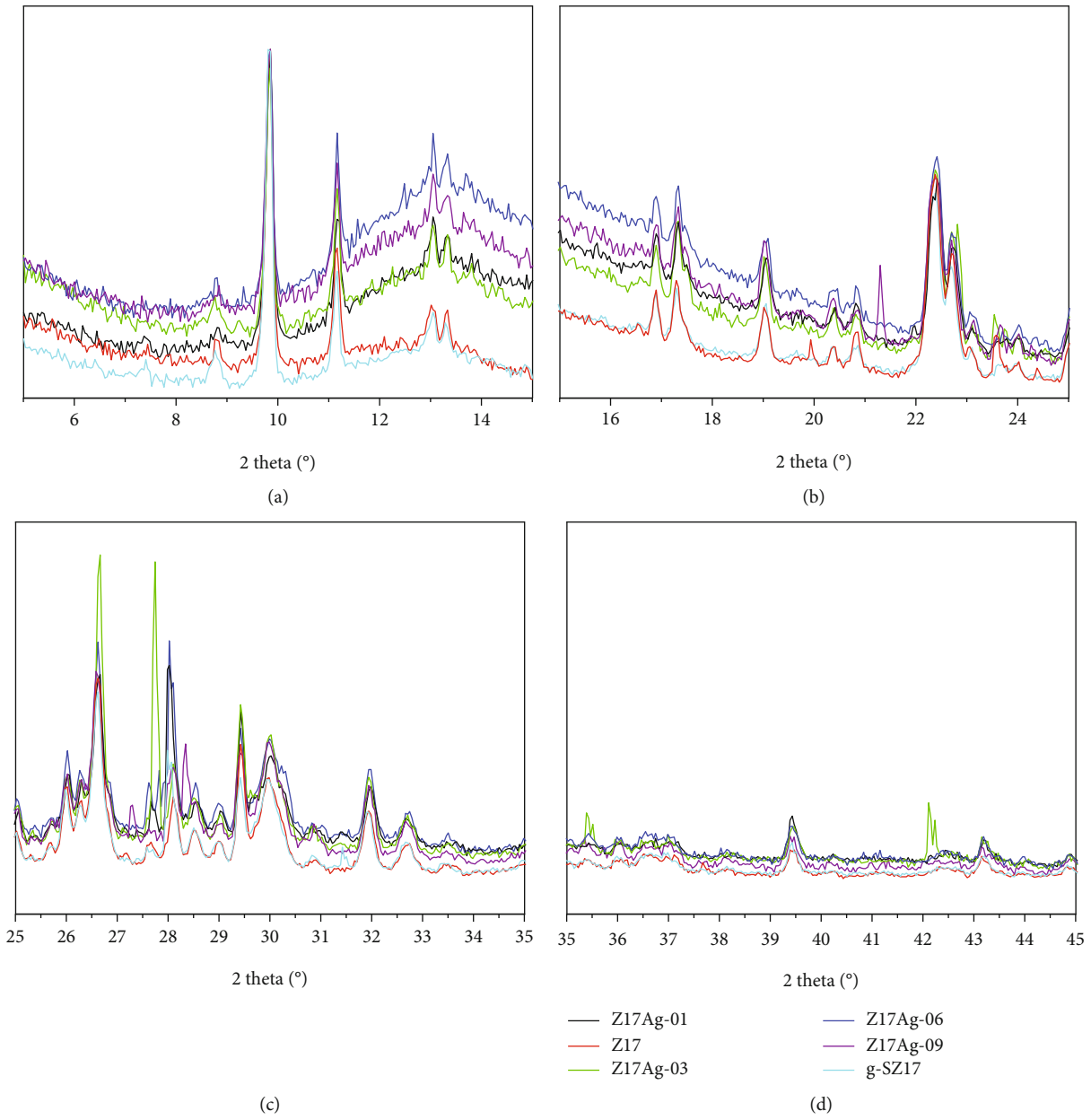

Figure 2: X-ray difraction of samples studied: (a) $2\theta = 5^{\circ}$-15°; (b) $2\theta = 15^{\circ}$-25°; (c) $2\theta = 25^{\circ}$-35°; (d) 35°-45°.

that previously reported [23]. The Mexican zeolitic mineral clinoptilolite from San Gabriel Chilac (Z17), Puebla, Mexico, was used in this work. The mineral clinoptilolite was powdered and sieved. Exchanged Ag-clinoptilolite samples Z17AgX were prepared from Z17 precursor and exchanged either $X = 1$, $X = 3$, $X = 6$, or $X = 9$ times with 0.01 N solutions of the corresponding cation salts ($AgNO_3$) at 298 K for 6 h. ROH, $AgNO_3$, and HCl of a commercial analytical grade were used without further purification. N_2 and He ultrahigh-purity gases (>99.999%, INFRA Corp.) were employed for the technique characterization of natural and chemically treated samples.

2.2. Methodology. The exchanged zeolite (Z17AgX) was dried at 423 K for 12 h. Subsequently, a mixture of ethanol was prepared with γ-SZ17 and Z17AgX in a 4 : 1 ratio, under rigorous stirring, and 373 K heat treatment was given for 12 h in order to evaporate the solvent.

2.3. Experimental Techniques

2.3.1. X-Ray Diffraction (XRD). Phase analysis by X-ray diffraction (Siemens D-500 X-ray Diffractometer) of samples was carried out at room temperature using CuKα as the radiation source at a scan speed of 0.5/min and a step scan of 0.02. The crystalline phase compositions were identified with reference to standard JCPDS cards available in the system software. The mean average crystalline size of exchanged Ag-clinoptilolite samples Z17AgX was calculated using Debye-Scherrer's equation [24].

Table 1: Origin and composition of phases for samples studied, XRD.

Sample	Location (town, state)	X-ray characterization (%)
Z17	San Gabriel Chilac, Puebla	Ca – clinoptilolite (~ 80) > quartz, calcite (~ 12.6) > mordenite (~ 8.8)

Table 2: Elemental chemical composition of studied samples, EDS.

Sample	Na	Mg	Al	Si	K	Ca	Ti	Fe	O	S	Ag	Si/Al	Total
γ-SZ17	2.63	1.10	6.30	34.30	1.46	3.55	0.22	1.75	48.69			5.444	100
Z17	2.81	0.86	6.34	34.96	1.35	3.10	0.12	1.24	49.12	0.10		5.514	100
Z17Ag01	2.00	0.83	6.50	34.40	1.24	3.82	0.13	0.94	48.47		1.67	5.292	100
Z17Ag03	1.16	0.96	6.28	33.02	1.43	3.93	0.13	1.23	46.91		4.94	5.257	100
Z17Ag06	1.81	0.93	6.32	33.78	1.48	4.34	0.14	1.25	47.97		1.98	5.344	100
Z17Ag09	1.31	0.88	6.12	33.56	1.26	4.26	0.12	1.25	47.40		3.83	5.810	100

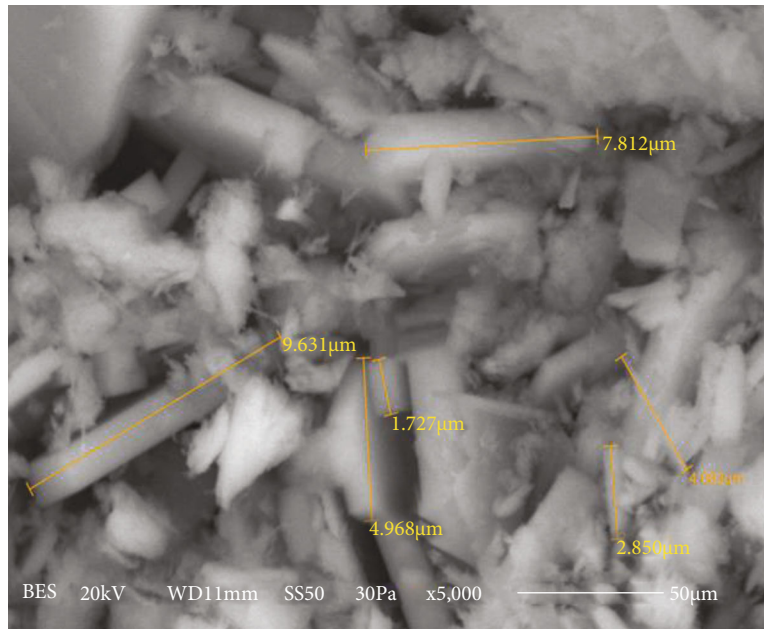

Figure 3: SEM images of Ca-clinoptilolite zeolite, Z17.

2.3.2. Fourier Transform Infrared Spectroscopy (FTIR). To obtain the infrared spectra, the infrared spectroscopy method with attenuated total reflectance accessory (ATR) was used. This method involves placing a sample on top of a crystal with a high refractive index. An infrared beam from the instrument is passed into the accessory and up into the crystal. It is then reflected internally in the crystal and back towards the detector which is housed in the instrument. When the beam is reflected within the crystal, it penetrates into the sample by a few microns.

2.3.3. Scanning of Electron Microscopy (SEM). Photomicrographs of samples under study were obtained with a Tescan Vega, model JSM-5300 scanning electron microscope. The samples were mounted on aluminium stubs and subsequently coated with Au/Pd using a sputter coater (Polarons SC 7610, Fision Instruments)

2.3.4. Energy Dispersive Spectroscopy (EDS). The chemical analyses were performed through EDS.

2.3.5. N_2 Adsorption. The N_2 sorption isotherms were measured at the temperature of 77 K (boiling temperature at altitude conditions of the City of Puebla, Mexico) in an automatic volumetric sorption instrument Quantachrome Autosorb-AS1. Isotherms were determined in the range of relative pressures $p/p^0 = 10^{-5} - 0.995$; the saturation pressure, p^0, was recorded continuously during the course of the adsorption measurements. Before starting the adsorption run, 60–80-mesh particles of each substrate were thoroughly degassed at 623 K for 20 h at a pressure lower than 10^{-6} mbar which was provided by the turbopump of the instrument. Textural results (surface areas and pore volumes) were obtained from pertinent analyses of the N_2 isotherms at 77 K; the following approaches were chosen to calculate the

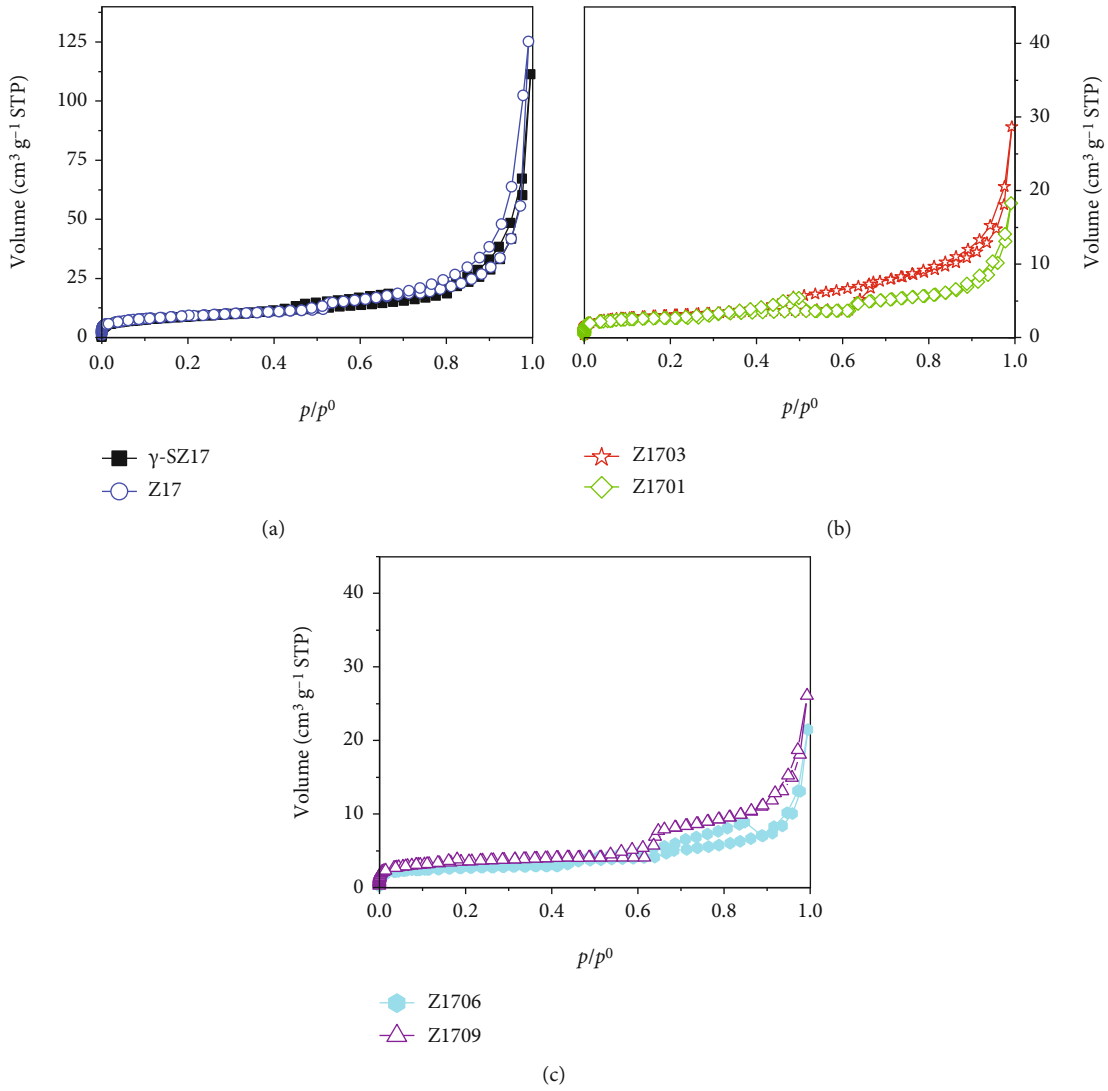

Figure 4: N_2 adsorption isotherms at 77 K on clinoptilolite zeolites exchanged.

desired textural properties: (i) the BET equation, (ii) the Langmuir equation, (iii) the *t*-plots for determining the external surface area, and (iv) the Gursvich rule to assess the total pore volume. The pore size distributions of the samples under study were evaluated from data of N_2 desorption isotherm by means of the BJH equation [25].

2.4. Antimicrobial Activity. As previously described [26], the Z17AgX antimicrobial activity was studied by performing an agar well diffusion method. This method was done against different bacterias, such as Gram-negative bacteria (*E. coli* ATCC 25922, *S. saprophyticcus* ATCC savage, *S. aureus* ATCC 29331, *S. epidermidis* ATCC 12228, and *E. feacalis* ATCC 29211) and Gram-positive bacteria (*P. aureoginosa* ATCC 27853, *K. pneumonie* ATCC 700603, and *A. baumannii*). Each sample was arranged by preparing, sterilizing, and solidifying each Mueller-Hinton agar plates. For every single bacterial strain, the samples were uniformly swabbed by sterile cotton swabs on the individual petri plates. By carrying out gel puncture, it was possible to prepare different wells of determined size. Into these wells, distinct concentrations of Z17AgX were filled up. The choosen concentrations were 0.010, 0.03, 0.06, and 0.09). Following this process, the plates were incubated for 24 h at 37°C. Subsequently, each plate was examined for a zone of incubation in millimeter.

3. Results and Discussion

3.1. XRD. The X-ray diffraction patterns of the samples obtained, Z17, Z17AgX, and the γ-sitoesterol-clinoptilolite (γ-SZ17) are presented in Figure 2. From this figure, different peaks are observed for each particular material. In the diffraction pattern corresponding to Z17Ag-03, signals located at $2\theta = 27.74^\circ$, 35.38°, 35.50°, 42.15°, and 42.20° stood out. These peaks can be attributable to the Ag incorporation into the zeolite framework [27, 28]. The average mean size of nanoparticles (AgNPs) was determined using Debye-Sherrer's equation. The size was estimated to be approximately 45.387 nm from the breadth of the reflection principal. As the size is considerably low, the AgNPs must be polycrystalline, and the single crystal shows higher size range [29, 30]. A

Table 3: Textural parameters of clinoptilolite zeolites exchanged determined from N_2 adsorption[a].

Sample	A_{SB} ($m^2 g^{-1}$)	C_B	A_{SL} ($m^2 g^{-1}$)	A_{St} ($m^2 g^{-1}$)	V_Σ ($cm^3 g^{-1}$)	Dp_{BJH} (nm)
γ-SZ17	31.2	142.4	39.9	25.5	0.0703	3.47
Z17	13.59	65	20.98	8.109	0.031	1.262/1.933/3.824/4.282
Z17Ag01	8.94	-199	12.37	2.731	0.0157	5.545/5.533
Z17Ag03	10.34	-610	15.88	6.682	0.028	NA
Z17Ag06	8.85	-179	13.09	4.742	0.0155	3.666/7.021
Z17Ag09	11.81	-41	17.69	4.906	0.0224	1.853/4.275/5.967

[a]A_{SB} is the specific surface area, BET equation; A_{SL} is the specific surface area, Langmuir equation; A_{St} is the external area, De Boer equation; C_B is the constant BET; V_Σ is the total pore volume, Gursvitch's rule; Dp_{BJH} is the pore diameter calculated by the BJH method.

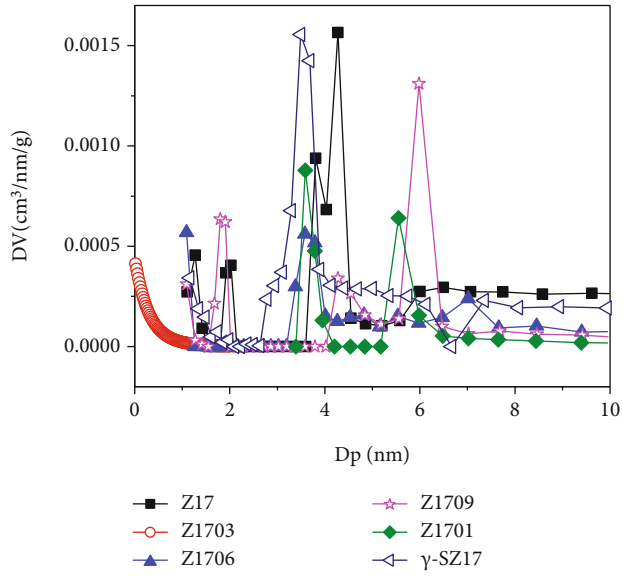

Figure 5: Pore size distribution of exchanged clinoptilolite zeolite, BJH method.

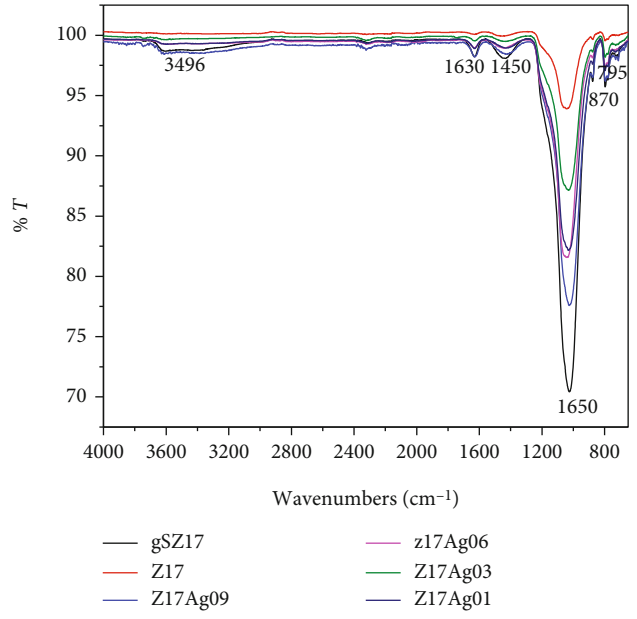

Figure 6: FTIR spectra of samples studied.

signal in $2\theta = 31.50^{\circ}$ is attributable to extract with γ-sitoesterol for sample γ-SZ17. This mark suggesting the bioorganic phase crystallization occurs on the surface of the silver nanoparticles. Similar results were found in silver nanoparticles synthesized by using edible mushroom extract [31, 32]. The signals corresponding to sample Z17 are located at the following $2\theta = 9.86^{\circ}$, 11.06°, 13.03°, 14.82°, 16.86°, 17.2°, 19.04°, 22.35°, 25.04°, 28.09°, 31.71°, and 32.67° (Figure 2). From this figure, it is observed the clinoptilolite signals prevail. The signals existing in the majority fundamentally correspond to the clinoptilolite zeolite (JCPDS 3 0427). Followed by small amounts of impurities such as montomorillonite (JCPDS 29-1498), quartz (2θ~27°, JCPDS 3-0427), and in some trace cases of mica, orthoclase, cristobalite, and magnesium calcite. These results were obtained by processing the diffraction patterns and the atomic coordinates of the phases present in each sample studied, using the High Score Plus 3.0e computer program, Table 1.

3.2. EDS. From the sequence of the zeolites studied, it is observed that in all the zeolites studied, they present a Si/Al molar ratio > 5. Based on this aspect, it can be assumed that this type of zeolites is the product of sediments from saline lakes and seas of these characteristics. It has been shown that, among zeolites of this type with a high amount of Si and with a molar ratio greater than 4, K-clinoptilolite zeolite predominates. This is due to the dominant rocks that are formed in deep water areas. However, Na-clinoptilolite and Ca-clinoptilolite zeolites can form under a wide group of parameters and appear in hydrothermal active systems of volcanic rocks, as well as in fractures and in internal cavities of these rocks. On the other hand, impurities associated with Fe^{3+}, which resides in the tetrahedral sites of this structure, can be associated with hematite impurities [33].

From the results reported in Table 2, the following sequences can be established: γ-SZ17: Ca > Na > Fe > K > Mg > Ti; Z17: Ca > Na > K > Fe > Mg > Ti > S; Z17Ag01: Ca > Na > Ag > K > Fe > Mg > Ti; Z17Ag03: Ag > Ca > K > Fe > Na > Mg > Ti; Z17Ag06: Ca > Ag > Na > K > Fe > Mg > Ti; and Z17Ag09: Ca > Ag > Na > K > Fe > Mg >Ti. It is observed from these results that for the samples exchanged with Ag, the following sequence is established: Z17Ag03>z1709>Z17Ag06>Z17Ag01 and Si/Al ratio es: Z17Ag09>Z17>γ-SZ17>Z17Ag06>Z17Ag01>Z17Ag03.

3.3. SEM. SEM images of clinoptilolite crystals at different approximations are shown in Figure 3. This figure shows the presence of crystals with irregular and poorly defined box shapes typical for this type of zeolites. Also, from this figure, the presence of a group of lamellar pores can be observed. On the other hand, at very low concentrations, the presence of Ag on Z17 (Ca-clinoptilolite) is not detected by SEM. However, this presence can be quantified through XRD and EDS (results presented in Table 2 and Figure 2). This effect has already been previously reported [34].

3.4. Adsorption of N_2. In Figure 4, the adsorption isotherms of N_2 at 77 K in the studied samples are observed (volume adsorbed, V, vs. relative pressure, p/p^0). This figure shows the formation of type II-IV isotherms within the IUPAC classification [25], for samples that are subjected to chemical treatments with $AgNO_3$. However, there is the formation of a stepped type VI isotherm for sample Z1709. The formation of a type H3 hysteresis cycle associated with the presence of pores in the form of sheets and/or lamellars is observed. The experimental points corresponding to the adsorption branch in areas of $p/p^0 < 0.05$-0.25 were evaluated by the Langmuir and BET equations. In the area of $p/p^0 = 0.1$-0.8, the experimental points were evaluated with the De Boer equation in order to evaluate the external area, A_{St}. At $p/p^0 \approx 0.95$, the total pore volume, V_{Σ}, was evaluated by means of Gursvitch's rule. On the other hand, the experimental points of desorption branches were considered for the evaluation of the pore size distribution

Table 4: Inhibition haloes produced in Gram-positive and Gram-negative strains in the presence of silver exchanged zeolites (Z17AgX) agar well diffusion method.

	Samples Z17Ag	Diameter of inhibition zones (mm)
Gram-positive strains		
P. aureoginosa	01	11
	03	11
	06	14
	09	15
K. pneumonie	01	10
	03	10
	06	11
	09	11
A. baumannii	01	11
	03	14
	06	16
	09	17
Gram-negative strains		
E. coli	01	10
	03	10
	06	12
	09	12
S. saprophyticcus	01	10
	03	10
	06	13
	09	13
S. aureus	01	11
	03	13
	06	14
	09	15
E. feacalis	01	—
	03	9
	06	11
	09	12

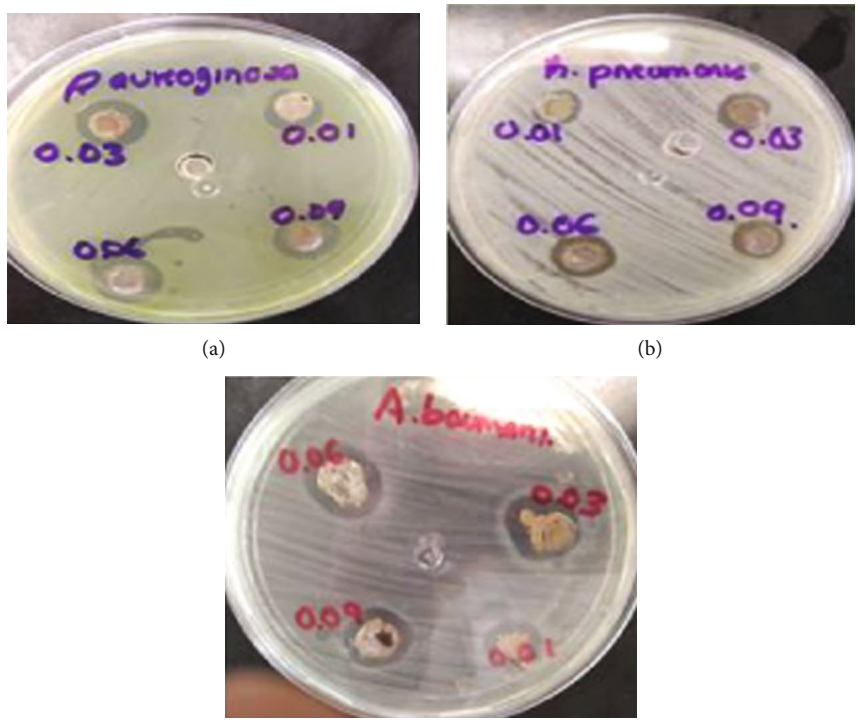

(a) (b) (c)

Figure 7: Antimicrobial susceptibility disk diffusion method. Gram-positive strains: (a) *P. aureoginosa*, (b) *K. pneumonie*, and (c) *A. baumannii*.

using the BJH equation. The results of these estimates are reported in Table 3.

From this table, it is observed that there is a decrease in the A_{SB} specific surface estimated by BET equation in the zeolite with chemical modification. This behavior of the chemically modified zeolites is associated with the existence of a blockage of the pores or channels. This blockage is caused by the organic γ-sitosterol (γ-SNPs) and inorganic silver nanoparticles (AgNPs), since their diameters and/or sizes are superior to the channels of the zeolite structure. On the other hand, it is observed that the values of the external area are considerable. The values of the external area are very important since it is in that area of the structure where the nanoparticles of γ-SNPs and AgNPs will be formed and stabilized. Figure 5 shows the curves calculated by the BJH method. In this figure, Z17 exhibits a sharp multimodal distribution with pore size maxima happening at 1.262, 1.933, 3.824, and 4.282 nm. For its part, Z17Ag01 exhibits a bimodal distribution with pore size maxima occurring at 5.45 and 5.533 nm. For Z17Ag03, representative pore size results could not be obtained by the BJH method because of the flat aspect of the resultant curve. In contrast, Z17Ag06 exhibits a sharp bimodal distribution with pore size maxima happening at 3.666 and 7.021 nm. Finally, the sample Z17Ag09 exhibits a sharp trimodal distribution with pore size maxima happening at 1.853, 4.275, and 5.967 nm, and these values are in the last column of Table 3.

3.5. Infrared Spectroscopy FTIR. In Figure 6, the IR spectra of the natural zeolite Z17; the zeolite treated with γ-sitosterol and γ-SZ17, and of the zeolites exchanged with Ag and Z17AgX are shown. Common bands are observed for all the samples studied. The wideband around 3496 cm^{-1} and 1630 cm^{-1}can be assigned to water molecules physisorbed in zeolites and for an internal tetrahedral asymmetric stretching O-H bending. The narrow band around 1450 cm^{-1} determined in the Ag-exchanged clinoptilolites is attributed to the presence of nitrates, which are located in the external area of the lattice corresponding to the exchanged clinoptilolite zeolites. The strong band 1050 cm^{-1} assigned to external tetrahedral linkage asymmetric stretching depends on Ag concentration on the external surface area of exchanged zeolites. The weak bands located at 870 and 795 cm^{-1} corresponds to external tetrahedral linkage symmetric stretching. These bands correspond to the Al-O-Si bonds present in the exchanged clinoptilolite zeolites [35].

3.6. Antibacterial Effect. The bacterecidal effect of the prepared samples (Z17AgX) were measured on Gram-negative and Gram-positive strains, Table 4, using disk diffusion method. The results obtained were compared among the samples prepared with Ag at different concentrations because both the Z17 precursor sample and the one γ-SZ17 gave an adverse result to this effect. The disk difusion method shows the magnitude of the susceptibility of the pathogenic microorganisms (Figures 7 and 8). The mean of three replicates of the diameter (in millimeters) of inhibition zones containing Z17AgX suspension is presented in Table 4. Among the Gram-positive strains, the samples Z17AgX show a bactericidal effect; however, the one with the greatest bactericidal

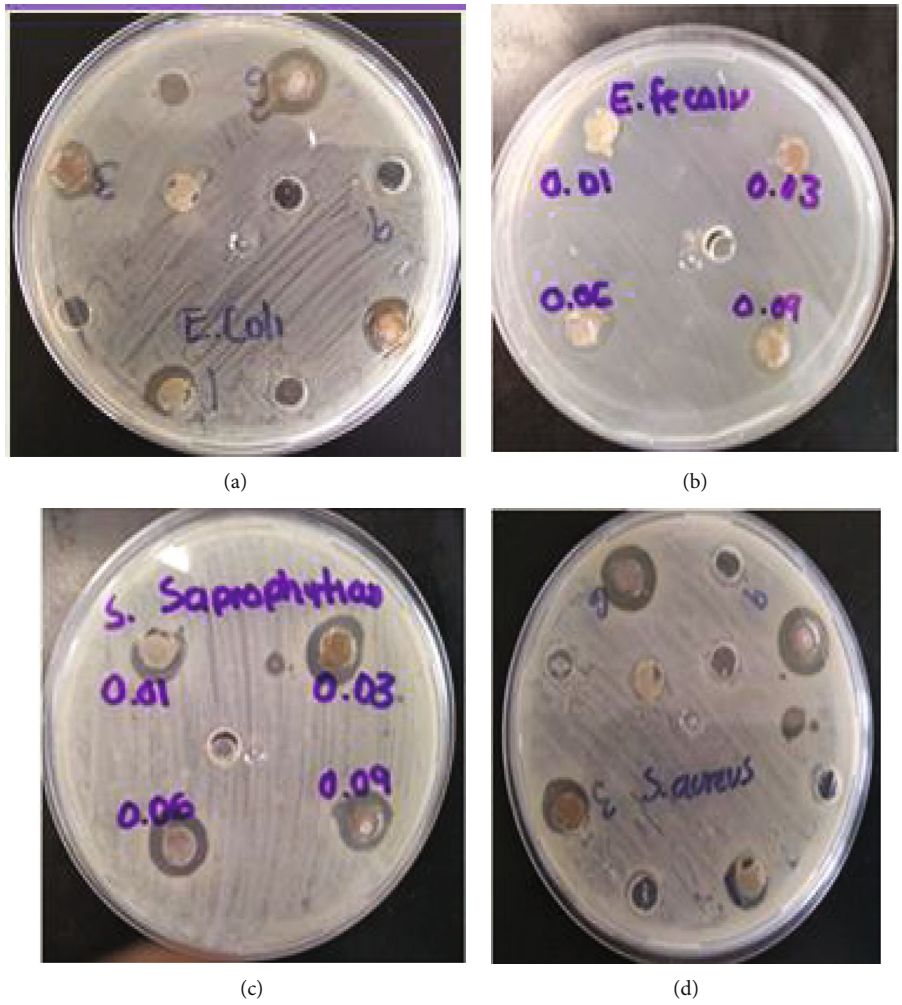

(a) (b) (c) (d)

Figure 8: Antimicrobial susceptibility disk diffusion method. Gram-negative strains: (a) *E. coli*, (b) *E. fecallis*, (c) *S. saprophyticcus*, and (d) *S. aureus*.

effect is sample Z17Ag09. The results of this behavior are presented in Table 4. From this table, the following sequence is established for Gram-positive strains present: *A. baumannii* (17 mm) > *P. aureoginosa* (15 mm) > *K. pneumonie* (11 mm). On the other hand, the results corresponding to the Gram-negative strains present the following sequence: *S. aureus* (15 mm) > *S. saprophyticcus* (13 mm) > *E. feacalis* (12 mm) = *E. coli* (12 mm). The results shown for the Z17AgX indicate that they are effective as antibacterial agents. Ag particles damage the cell walls and membranes of pathogenic bacteria, inhibiting enzymatic activity and bacterial replication. Ag cations are microbicidal at low concentrations and do not have major side effects in humans [2].

4. Conclusions

Clinoptilolite-rich minerals from San Juan Gabril Chilac, Puebla, Mexico, and those of modified forms were characterized by using XRD, SEM, EDS, and nitrogen adsorption analysis techniques. Based on the X-ray analysis, the purity percentage of the crystalline phases constituting the original zeolitehas been established. For Z17: Ca-clinoptilolite (~80) > quartz, calcite (~12.6) > mordenite (~8.8). Additionally, X-ray analysis of the zeolite samples has shown that the modification of clinoptilolites with a solution of $AgNO_3$ and γ-sitosterol does not lead to significant structural changes. The organic (γ-sitosterol) and inorganic (Ag^{+1}) nanoparticles form nanoparticles in the external area of the clinoptilolite zeolite. Their degree of dispersion and stabilization is a function of the external area developed, as well as the zeolite degree of mesoporosity. From the results shown above, it can be concluded that AgZ1709 exchanged zeolite is the most promising material as a microbicidal agent, which in combination with γ-SZ17 would be recommended for its application in diabetic foot treatments.

Data Availability

No data were used.

Conflicts of Interest

The authors declare no conflict of interest.

Authors' Contributions

All authors discussed and agreed upon the idea and made scientific contributions: writing and original draft preparation, MAH; experiment designing, MA and GIH; experiment performing, RP; data analysis, ER; writing, review, and editing, MAS and VP. All authors have read and agreed to the published version of the manuscript.

Acknowledgments

This work was supported by the VIEP and the Academic Body "Investigación en zeolitas" (CA-95) (PROMEP-SEP).

References

[1] J. Hardwicke, R. Moseley, P. Stephens, K. Harding, R. Duncan, and D. W. Thomas, "Bioresponsive dextrin–rhEGF conjugates: in vitro evaluation in models relevant to its proposed use as a treatment for chronic wounds," *Molecular Pharmaceutics*, vol. 7, no. 3, pp. 699–707, 2010.

[2] J. Milenkovic, J. Hrenovic, D. Matijasevic, M. Niksic, and N. Rajic, "Bactericidal activity of Cu-, Zn-, and Ag-containing zeolites toward *Escherichia coli* isolates," *Environmental Science and Pollution Research*, vol. 24, no. 25, pp. 20273–20281, 2017.

[3] D. Barathi, S. Vasantharaj, and V. Bhuvaneshwari, "Green synthesis of silver nanoparticles using Cordia dichotoma fruit extract and its enhanced antibacterial, anti-biofilm and photo catalytic activity," *Materials Research Express*, vol. 5, no. 5, article 055404, 2018.

[4] D. Barathi and V. Bhuvaneshwari, "Evaluation of the cytotoxic and antioxidant activity of phyto-synthesized silver nanoparticles using Cassia angustifolia flowers," *BioNanoScience*, vol. 9, no. 1, pp. 155–163, 2019.

[5] Y. Wu, Y. Yang, Z. Zhang, Z. Wang, Y. Zhao, and L. Sun, "A facile method to prepare size-tunable silver nanoparticles and its antibacterial mechanism," *Advanced Powder Technology*, vol. 29, no. 2, pp. 407–415, 2018.

[6] Z. Ni, Z. Wang, L. Sun, B. Li, and Y. Zhao, "Synthesis of poly acrylic acid modified silver nanoparticles and their antimicrobial activities," *Materials Science and Engineering C*, vol. 41, pp. 249–254, 2014.

[7] L. G. Rossainz-Castro, I. de-la-Rosa-Gómez, T. Olguín, and D. Alcántara-Díaz, "Comparison between silver- and copper-modified zeolite-rich tuffs as microbicide agents for *Escherichia coli* and *Candida albicans*," *Journal of Environmental Management*, vol. 183, Part 3, pp. 763–770, 2016.

[8] J. Hrenovic, J. Milenkovic, T. Ivankovic, and N. Rajic, "Antibacterial activity of heavy metal-loaded natural zeolite," *Journal of Hazardous Materials*, vol. 201-202, pp. 260–264, 2012.

[9] F. A. Mumpton, "La roca magica: uses of natural zeolites in agriculture and industry," *Proceedings of the National Academy of Sciences of the United States of America*, vol. 96, no. 7, pp. 3463–3470, 1999.

[10] G. V. Tsitsihvili, T. G. Andronikashvili, G. N. Kirov, and N. Filizova, *Natural Zeolites*, Ellis Horwood, Chichester, UK, 1992.

[11] A. Semra and U. Semra, "Ag, Zn, and Cu exchange in a Na-clinoptilolite and resulting effect on antibacterial activity," *Applied Clay Science*, vol. 27, pp. 13–19, 2004.

[12] L. Dimova, O. Petrov, M. Kadiyski, N. Lihareva, A. Stoyanova-Ivanova, and V. Mikli, "Preparation and Rietveld refinement of Ag-exchanged clinoptilolite," *Clay Minerals*, vol. 46, no. 2, pp. 205–212, 2011.

[13] B. Concepcion-Rosabal, G. Rodriguez-Fuentes, and R. Simon-Carballo, "Development and featuring of the zeolitic active principle FZ: a glucose adsorbent," *Zeolites*, vol. 19, no. 1, pp. 47–50, 1997.

[14] G. Rodriguez-Fuentes, M. A. Barrios, A. Iraizoz, I. Perdomo, and B. Cedre, "Enterex: anti-diarrheic drug based on purified natural clinoptilolite," *Zeolites*, vol. 19, no. 5-6, pp. 441–448, 1997.

[15] N. Bogdanchikova, B. Concepcion-Rosabal, V. Petranovskii, M. Avalos-Borja, and G. Rodriguez-Fuentes, "Microbicide effect of Ag-clinoptilolites: I. Preparation and investigation of structure of samples containing silver in different states," *Proceedings SPIE 4097, Complex Mediums*, 2000.

[16] B. Concepcion-Rosabal, G. Rodrıguez-Fuentes, N. Bogdanchikova, P. Bosch, M. Avalos, and V. H. Lara, "Comparative study of natural and synthetic clinoptilolites containing silver in different states," *Microporous and Mesoporous Materials*, vol. 86, no. 1-3, pp. 249–255, 2005.

[17] S. K. Pavelic, J. S. Medica, D. Gumbarevic, A. Filosevic, N. Przulj, and K. Pavelic, "Critical review on zeolite clinoptilolite safety and medical applications in vivo," *Frontiers in Pharmacology*, vol. 9, article 1350, pp. 1–15, 2018.

[18] C. Colella, "Natural zeolites in environmentally friendly processes and applications," *Studies in Surface Science and Catalysis*, vol. 125, pp. 641–655, 1999.

[19] C. Colella, "A critical reconsideration of biomedical and veterinary applications of natural zeolites," *Clay Minerals*, vol. 46, no. 2, pp. 295–309, 2011.

[20] G. Cerria, M. Gennaro, M. C. de Bonferoni, and C. Caramella, "Zeolites in biomedical application: Zn-exchanged clinoptilolite-rich rock as active carrier for antibiotics in *anti-acne* topical therapy," *Applied Clay Science*, vol. 27, no. 3-4, pp. 141–150, 2004.

[21] N. Triphathi, S. Kumar, R. Singh, C. J. Singh, P. Singh, and V. K. Varshney, "Isolation and identification of gamma-sitosterol by GC-MS from roots of Girardinia heterophylla," *Oriental Journal of Chemistry*, vol. 29, no. 2, pp. 705–707, 2013.

[22] R. Balamurugan, V. Duraipandiyan, and S. Ignacimuthu, "Antidiabetic activity of γ-sitosterol isolated from Lippia nodiflora L. in streptozotocin induced diabetic rats," *European Journal of Pharmacology*, vol. 667, no. 1-3, pp. 410–418, 2011.

[23] M. A. Hernandez, F. Rojas, and M. A. Salgado, "Nanopore organic-inorganic hybrid materials with properties of cell regeneration I. Physicochemical and morphological characterization," *MRS Online Proceedings Library*, vol. 1487, pp. 39–45, 2012.

[24] M. Vanaja and G. Annadural, "Coleus aromaticus leaf extract mediated synthesis of silver nanoparticles and its bactericidal activity," *Applied Nanoscience*, vol. 3, no. 3, pp. 217–223, 2013.

[25] M. Thommes, K. Kaneko, A. V. Neimark et al., "Physisorption of gases, with special reference to the evaluation of surface area and pore size distribution (IUPAC technical report)," *Pure and Applied Chemistry*, vol. 87, no. 9-10, pp. 1051–1069, 2015.

[26] K. Gudikandula and S. Charya Maringanti, "Synthesis of silver nanoparticles by chemical and biological methods and their

antimicrobial properties," *Journal of Experimental Nanoscience*, vol. 11, no. 9, pp. 714–721, 2016.

[27] D. Philip, "Biosynthesis of Au, Ag, and Au-Ag nanoparticles using edible mushroom extract," *Spectrochimica Acta Part A*, vol. 7, pp. 374–381, 2009.

[28] S. Sharkar, A. Ahmad, and M. Sastry, "Geranium leaf assisted biosynthesis of silver nanoparticles," *Biotechnology Progress*, vol. 19, no. 6, pp. 1627–1631, 2003.

[29] D. Barathi, M. D. Josebin, S. Vasantharaj, and V. Bhuvaneshwari, "Biosynthesis of silver nanoparticles using stem bark extracts of Diospyros montana and their antioxidant and antibacterial activities," *Journal of Nanostructure in Chemistry*, vol. 8, no. 1, pp. 83–92, 2018.

[30] B. Das, S. K. Dash, D. Mandal et al., "Green synthesized silver nanoparticles destroy multidrug resistant bacteria via reactive oxygen species mediated membrane damage," *Arabian Journal of Chemistry*, vol. 10, no. 6, pp. 862–876, 2017.

[31] L. Akhigbe, S. Ouki, D. Saroj, and X. M. Lim, "Silver-modified clinoptilolite for the removal of Escherichia coli and heavy metals from aqueous solutions," *Environmental Science and Pollution Research*, vol. 21, no. 18, pp. 10940–10948, 2014.

[32] S. Demirci, Z. Ustaoğlu, G. A. Yılmazer, F. Sahin, and N. Baç, "Antimicrobial properties of zeolite-X and zeolite-a ion-exchanged with silver, copper, and zinc against a broad range of microorganisms," *Applied Biochemistry and Biotechnology*, vol. 172, no. 3, pp. 1652–1662, 2014.

[33] A. Mastinu, A. Kumar, G. Maccarinelli et al., "Zeolite clinoptilolite: therapeutic virtues of an ancient mineral," *Molecules*, vol. 24, no. 8, pp. 1517–1531, 2019.

[34] M. A. Hernández, F. Rojas, R. Portillo, M. A. Salgado, V. Petranovskii, and K. Quiroz, "Textural Properties of Hybrid Biomedical Materials Made from Extracts of Tournefortia hirsutissima L. Imbibed and Deposited on Mesoporous and Microporous Materials," *Journal of Nanomaterials*, vol. 2016, Article ID 1274817, 10 pages, 2016.

[35] W. Mozgawa, M. Krol, and K. Barczyk, "FT-IR studies of zeolites from different structural groups," *Chemik*, vol. 65, pp. 667–674, 2011.